JACS
JOURNAL OF THE AMERICAN CHEMICAL SOCIETY
Article
pubs.acs.org/JACS

Tuning the Surface Chemistry of Metal Organic Framework Nodes: Proton Topology of the Metal-Oxide-Like Zr_6 Nodes of UiO-66 and NU-1000

Dong Yang,[†] Varinia Bernales,[‡] Timur Islamoglu,[§] Omar K. Farha,[§,∥] Joseph T. Hupp,[§] Christopher J. Cramer,[‡] Laura Gagliardi,*[,‡] and Bruce C. Gates*[,†]

[†]Department of Chemical Engineering, University of California, Davis, California 95616, United States
[‡]Department of Chemistry, Chemical Theory Center, and Supercomputing Institute, University of Minnesota, Minneapolis, Minnesota 55455-0431, United States
[§]Department of Chemistry, Northwestern University, 2145 Sheridan Road, Evanston, Illinois 60208, United States
[∥]Department of Chemistry, Faculty of Science, King Abdul-Aziz University, Jeddah 22254, Saudi Arabia

Supporting Information

ABSTRACT: Some metal organic frameworks (MOFs) incorporate nodes that are nanoscale metal oxides, and the hydroxy-containing functional groups on them provide opportunities for introducing catalytic sites with precisely defined structures. Investigations have been done to understand the structures of these groups on nodes and node vacancies, because, in prospect, atomic-scale modulation of the composition, areal density, and/or siting of the groups would open up possibilities for exquisite tuning of the siting and performance of subsequently anchored catalytic units (e.g., single metal ions, pairs of metal ions, or well-defined metal-ion-containing clusters). We have combined infrared (IR) spectroscopy and density functional theory (DFT) to demonstrate tuning of these sites, namely, hydrogen-bonded OH/OH_2 groups on the Zr_6 nodes of the MOFs UiO-66 and NU-1000 via the intermediacy of node methoxy (or ethoxy) groups formed from methanol (or ethanol). Methoxy (or ethoxy) groups on node vacancy sites are converted to a structure incorporating one vacant Zr site and one terminal OH group per face by reaction with water. Our results highlight how the combination of DFT and IR spectroscopy facilitates the determination of the identity and chemistry of the functional groups on MOF node vacancies and defect sites.

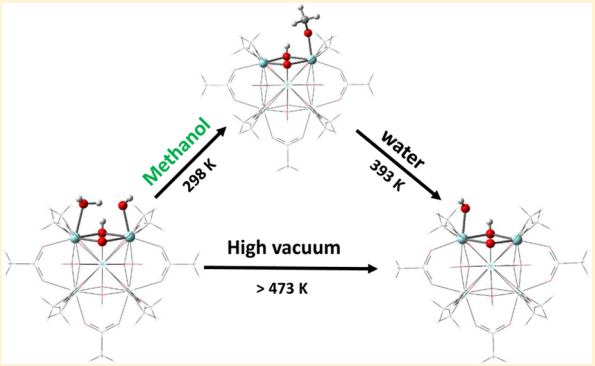

INTRODUCTION

The nodes of some metal−organic frameworks (MOFs) are essentially small, uniform metal oxide clusters, exemplified by the Zr_6 nodes of UiO-66,[1] UiO-67,[1] and NU-1000.[2] The strong coordination bonds between these nodes and carboxylate oxygen atoms in the linkers help to stabilize these MOFs, which can be used at high temperatures (in the range 300−400 °C[3]) and are therefore attractive in prospect for applications as catalysts and catalyst supports. The crystal structures of these MOFs have been determined by X-ray diffraction crystallography,[1,2] but this technique is not sufficient to determine the identities and placement of small *non*-structural ligands (i.e., ligands other than linkers) such as hydroxyl and aqua groups on the nodes.

The nonstructural ligands on the nodes of UiO-66 and UiO-67 are associated with missing linkers[4,5] (and, in some cases, nodes[6−8]). The nodes of UiO-type MOFs are nominally (or ideally) 12-linker-connected, but in real samples, the number is less. The hexa-metal(IV) nodes of NU-1000, in contrast, are inherently 8- rather than 12-connected, thus leaving numerous sites for binding of nonstructural ligands, even in the absence of structural defects.[5] The node-ligated aqua and hydroxo species are Brønsted acids[9,10] comparable to those on the surfaces of metal oxides and zeolites, and the corresponding MOFs are therefore comparable to these materials as catalysts and catalyst supports, albeit with potentially different properties owing to the nanoscale of the nodes and/or local confinement by the framework.

Because MOFs in prospect have structures that can be tuned more precisely than those of metal oxides and even zeolites, they offer excellent opportunities to create unique, uniform surface sites that exhibit new, controllable reactivities and catalytic properties—and, correspondingly, they offer additional opportunities for the anchoring of unique catalytic sites such as metal complexes.[4,5,11−13] Therefore, there is a strong incentive

Received: August 8, 2016
Published: October 28, 2016

DOI: 10.1021/jacs.6b08273
J. Am. Chem. Soc. 2016, 138, 15189−15196

for investigating the precise molecular structures of MOF nodes and their vacancies, and for tailoring them when possible for specific functions, a subject that is still at an early stage of investigation. An important recent contribution in this respect is the work of Ling and Slater,[14] who investigated the dynamic acidity and interconversion of alternative defect terminations of UiO-66 in aqueous solution, extending the understanding[15] with respect to the proton topology of such node faces in water.

Using a combination of infrared (IR) spectroscopy and density functional theory (DFT) calculations,[16] we previously inferred that the NU-1000 nodes and their proton topology are well represented as $[Zr_6(\mu_3\text{-}O)_4(\mu_3\text{-}OH)_4(OH)_4(OH_2)_4]^{8+}$, with each structural vacancy occupied by a combination of terminal OH and OH_2 groups at sites referred to as **site 1** (Scheme 1). This same terminating functionality was also

Scheme 1. Simplified Depictions of the Zr_6 Node-Face Topologies, Site 1 and Site 2, the Latter Both as Originally Assigned and as Reassigned Here in Light of New Results, for the MOFs UiO-66 and NU-1000[a]

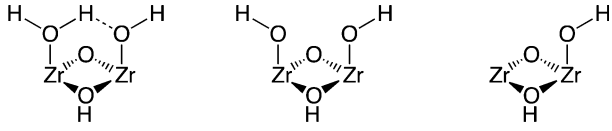

site 1 | **site 2** *originally assigned* | **site 2** *here reassigned*

[a]Note that the originally assigned **site 2** was for a Zr_6 node with the otherwise "missing" proton from **site 1** moved to another face of the core (i.e., all of the sites in this scheme have zero net charge and spin).

identified at the missing linker sites of UiO-66 and UiO-67 nodes.[4] Moreover, a second topology was observed for the nodes of UiO-66 and designated in the earlier work[4,5] as **site 2**. The topology for **site 2** was originally assigned as a node face having a pair of terminal OH groups, as illustrated in Scheme 1. The chemistries of these two sites were investigated in experiments with iridium carbonyl complexes as probes, and the chemisorbed iridium carbonyls were characterized by extended X-ray absorption fine structure (EXAFS) and IR spectra, with the latter demonstrating different electron-donor properties of the two distinct sites.[4,5]

An open challenge is to tune those groups terminating defects or vacancies on MOF node faces. Methods for interconverting such groups on individual faces are lacking and would be of particular value to the extent that they might modulate the properties of nodes and their reactivities for applications in catalysis and adsorption.

Carboxylate-containing functional groups[17,18] or, alternatively, phosphonate groups[19] have been reported to reactively replace the hydroxyl groups on the Zr_6 nodes through a solvent-assisted ligand incorporation (SALI) method. We now report how to incorporate methoxy ligands on the node surfaces and through their intermediacy to convert MOF node **site 1** into the alternative MOF node **site 2**. Importantly, we here reassign the nature of **site 2** to involve only a single terminating OH group together with a vacant Zr coordination site. Our results demonstrate a facial ligand exchange on the vacancies of these metal-oxide-like MOF nodes and indicate a subtlety in the acid−base properties of the nodes akin to that noted by Ling and Slater.[14]

EXPERIMENTAL AND COMPUTATIONAL METHODS

Synthesis of UiO-66. $ZrCl_4$ (99.99%, 0.125 g, 0.54 mmol) and 1 mL of concentrated HCl modulator (37 wt %, Sigma-Aldrich) were dissolved in 15 mL of dimethylformamide (DMF, 99.8%, Sigma-Aldrich) in an 8-dram vial by using ultrasound for 5 min. The linker precursor benzene-1,4-dicarboxylic acid (0.123 g, 0.75 mmol, ≥98.0%, Sigma-Aldrich) was dissolved in the solution with ultrasound applied for about 15 min. The vials were stored at 353 K for 24 h. The white precipitates that formed were isolated by centrifugation after cooling of the samples to room temperature. The solids were washed with DMF three times to remove unreacted precursors and with acetone six times to remove DMF, and the powder was then dried at room temperature.

Post Treatment of UiO-66 in Methanol. UiO-66 (20 mg) was placed in 2 mL of methanol (≥99.9%, Sigma-Aldrich, for HPLC) at 298 K and held for 48 h. The solution was decanted and replaced three times over the course of the experiment. The powder was dried in air at 298 K for 30 min. The residual methanol was then removed by treatment under dynamic vacuum overnight at 423 K.

Synthesis of NU-1000. A sample consisting of 97 mg of $ZrOCl_2 \cdot 8H_2O$ (0.30 mmol, 98.0%, Sigma-Aldrich) and 2700 mg (22 mmol) of benzoic acid (≥99.5%, Sigma-Aldrich) was mixed with 8 mL of DMF in a 6-dram vial and ultrasonically dissolved. The clear solution was incubated at 353 K for 1 h. After cooling of the solution to room temperature, 40 mg (0.06 mmol) of 1,3,6,8-tetrakis(*p*-benzoic acid)pyrene (H_4TBAPy[20]) was added, and the mixture was sonicated for 20 min. The yellow suspension was held at 353 K for 24 h. After cooling of the sample to room temperature, a yellow polycrystalline material was isolated by filtration (35 mg of activated material, 54% yield) and washed with DMF and then activated with HCl. The solid was subsequently washed twice with DMF and six times with acetone. The powder was dried at room temperature.

Post Treatment of NU-1000 in Methanol. NU-1000 (20 mg) was placed in 2.0 mL of methanol (≥99.9%, Sigma-Aldrich, for HPLC) at 343 K and held for 48 h. The solution was decanted and replaced three times over the course of the experiment. The methanol was then removed by treatment under dynamic vacuum at 298 K, and the sample was activated under dynamic vacuum at 423 K for 12 h.

IR Spectroscopy. A Bruker IFS 66v/S spectrometer with a spectral resolution of 2 cm^{-1} was used to collect transmission IR spectra of powder samples. Approximately 30 mg of solid sample in an argon-filled glovebox was pressed into a thin wafer and loaded into a cell that served as a flow reactor (In-situ Research Institute, South Bend, IN). The cell was sealed and connected to a flow system that allowed recording of spectra while reactant gases flowed through the cell at reaction temperature. Each spectrum is the average of 64 scans.

Isotopic Exchange Experiments. UiO-66 (20 mg) was placed in 2.0 mL of methanol-D_4 (99.5%, Cambridge Isotope Laboratories) and held at 293 K for 48 h. The solution was decanted and replaced three times over the course of the experiment. The methanol-D_4 was removed by evacuation by treatment under dynamic vacuum overnight at 423 K.

Models and Computational Details. *Cluster Model: NU-1000.* Calculations were performed starting from the mix-S topology of the Zr_6-NU-1000 node, $[Zr_6(\mu_3\text{-}O)_4(\mu_3\text{-}OH)_4(OH)_4(OH_2)_4]^{8+}$, reported by Planas et al.[16] The Zr_6 node of NU-1000 was modeled as a finite cluster extracted from an optimized periodic unit cell to allow a detailed investigation of the plausible new topologies of NU-1000.[16] The UiO-66/67 cluster model was obtained from Yang et al.,[4] with the organic linkers kept as acetate ($CH_3CO_2^-$) groups as in our previous studies (Figure 1).[4,16] Moreover, CM5 partial atomic charges[21] were computed for **site 1**, **site 2**, and other relevant structures (Table S2).

Kohn−Sham Density Functional Calculations. Clusters were optimized using the M06-L[22] density functional as implemented in the Gaussian 09 software package,[23] together with the def2-TZVP[24,25] basis set for C, H, O, and Zr atoms. Associated effective core potentials were used on Zr atoms. In all cases, the positions of all atoms were optimized, except for the C and H atoms of the capping acetate groups. The nature of all stationary points was verified by analytical

DOI: 10.1021/jacs.6b08273
J. Am. Chem. Soc. 2016, 138, 15189−15196

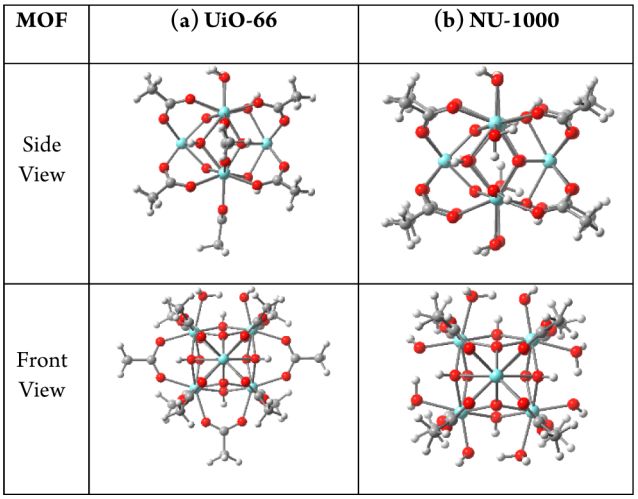

Figure 1. Schematic representation of the acetate cluster model used to calculate various topologies for (a) UiO-66 and (b) NU-1000. color Code: carbon, gray; hydrogen, white; zirconium, cyan; oxygen, red.

computation of vibrational frequencies, which were also used to compute 298.15 and 343 K thermochemical quantities with all frequencies below 50 cm^{-1} replaced by 50 cm^{-1} when computing free energies. The SMD continuum solvation model was employed to account for methanol solvation effects when comparing calculated results with those of experiments done in bulk solution,[26] except for water and methanol themselves as solutes, for which experimental values/estimates were employed. For details, see the Supporting Information.

RESULTS

The IR spectrum of a UiO-66 sample prepared in a synthesis modulated by HCl[4,27] and washed with acetone as shown in Figure 2. The band at 2746 cm^{-1} has been assigned to the hydrogen-bonded OH/OH_2 pairs of **site 1** on the Zr_6 node; the sharp band at 3674 cm^{-1}, with two weak shoulders, at 3688 and 3636 cm^{-1}, derives from a combination of the non-hydrogen-bonded OH groups of **site 1** together with the (perforce, also non-hydrogen-bonded) μ_3-OH bands,[4,16] with the majority of the intensity of the 3674 cm^{-1} band coming from the terminal groups (*vide infra*).

In the first step to generate **site 2** in this work, UiO-66 (modulated by HCl and washed with acetone) was treated in liquid methanol for 48 h at 298 K, followed by decanting of the methanol and drying of the sample at 298 K for 30 min, followed by activation under high vacuum at 423 K for 12 h to remove residual methanol. Analysis indicated that **site 1** was completely removed from the nodes after the treatment, as evidenced by the disappearance of the 2746 cm^{-1} band and a marked decrease in intensity of the 3674 cm^{-1} band (that component associated with the terminating groups, *vide supra*), with a concomitant growth of new bands at 2932 and 2828 cm^{-1} (Figure 2). These two new bands are consistent with the C−H stretches of methoxy groups.

It has correspondingly been reported that methanol reacts with the surface hydroxyl groups of bulk zirconia powder to form a methoxy-terminated surface accompanied by the release of water,[28,29] with the $Zr-OCH_3$ species exhibiting IR bands at 2923 and 2817 cm^{-1}. Similarly, methoxy groups on other metal oxides have been characterized by IR bands, at 2960 and 2849 cm^{-1} for Al_2O_3,[30] 2920 and 2815 cm^{-1} for Fe_2O_3,[31] and 2958 and 2858 cm^{-1} for SiO_2.[32]

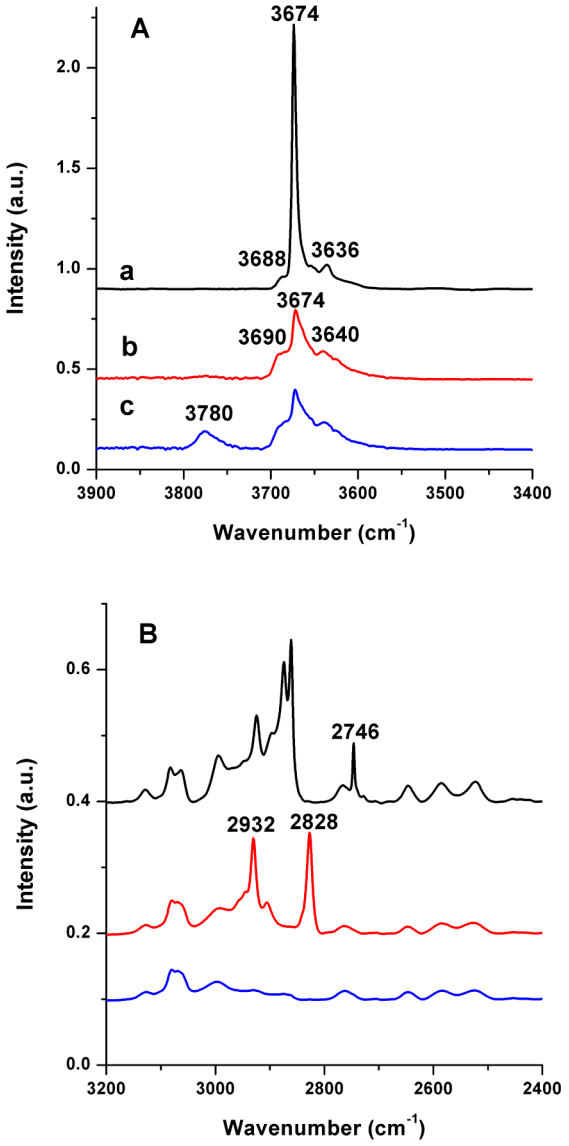

Figure 2. IR spectra in the (A) 3400−3900 cm^{-1} region and (B) 2400−3200 cm^{-1} region characterizing (a) UiO-66 and (b) UiO-66 after treatment in liquid methanol at 298 K for 48 h and (c) UiO-66 after treatment in water vapor/helium at 393 K for 30 min. The UiO-66 samples before and after treatment with liquid methanol or water vapor were activated at 393 or 423 K, respectively, by treatment under high vacuum for 12 h.

We thus infer that methanol reacts similarly with the hydroxyl groups of MOF **site 1** of UiO-66 to form $Zr-OCH_3$ at the missing linker sites. To check the assignment, the sample after methanol treatment and activation was immersed in excess methanol-D_4 at 298 K for 48 h. After the ensuing isotopic exchange, the bands at 2932 and 2828 cm^{-1} had disappeared, with the simultaneous growth of a sharp new band at 2060 cm^{-1} (Supporting Information, Figure S1). The frequency of this band agrees well with that of the IR band at 2062 cm^{-1} observed for $Zr-OCD_3$ on zirconia powder.[33]

We attempted to carry out the same conversion with UiO-67 but found that this MOF is not stable under the methanol treatment conditions. After 2 h of soaking in methanol, the UiO-67 completely lost its crystallinity.[4]

To check our ability to identify any physisorbed (as opposed to chemisorbed) methanol on the UiO-66 (and to exclude the

DOI: 10.1021/jacs.6b08273
J. Am. Chem. Soc. 2016, 138, 15189−15196

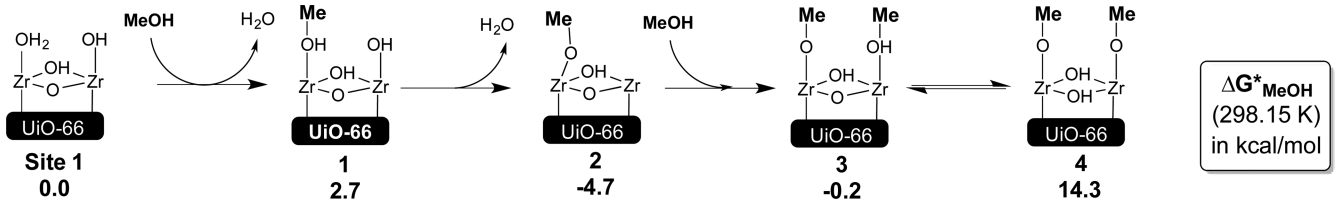

Figure 3. Relative free energies in kcal/mol (298.15 K, liquid methanol containing 1% H_2O) of possible products from methanol substitution.

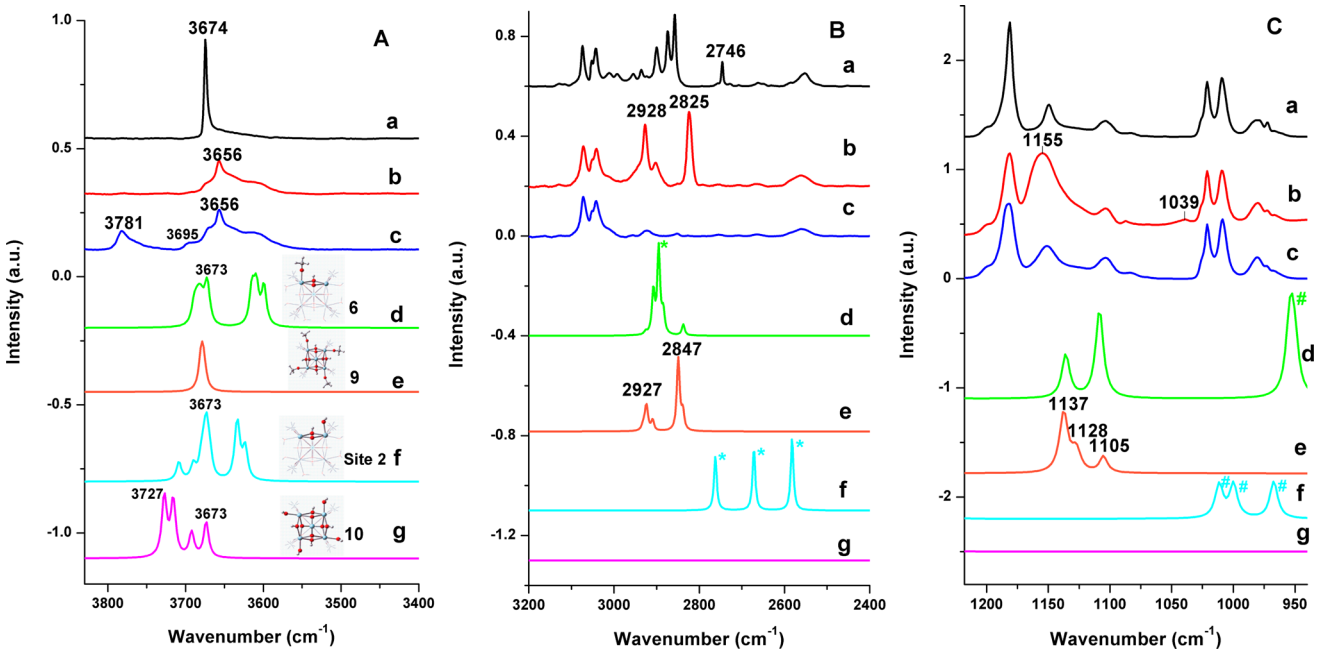

Figure 4. Experimental IR spectra (A) in the 3400−3900 cm^{-1} region, (B) in the 2400−3200 cm^{-1} region, and (C) in the 940−1250 cm^{-1} region characterizing NU-1000 (a), NU-1000 after treatment with liquid methanol at 343 K for 48 h (b), and the sample depicted in b after contact with water vapor/helium at 393 K for 30 min (c). NU-1000 and NU-1000 after treatment with liquid methanol were activated at 393 or 423 K, respectively, under high vacuum for 12 h. Theoretical IR spectra of model **6** (d), **9** (e), **site 2** (f), and **10** (g) in the C−H and O−H stretching regions. The bands were scaled with a factor of 0.958. Bands labeled with a pound symbol represent bonding of aqua ligands. We emphasize that each theoretical calculation is useful for assigning specific, cumulative changes in spectra, but that a direct comparison of theory with experiment is possible only between (b) and (e) and between (c) and (g), and even for these pairs, peaks associated with linker modes (e.g., C−H bond stretches) will not be found in the theoretical spectra. Color code: carbon, gray; hydrogen, white; zirconium, cyan; oxygen, red.

possibility of its presence in the aforementioned samples), the methanol-reacted UiO-66 was brought into contact with a pulse of methanol in helium at 373 K (~100 molecules per MOF node; methanol vapor was introduced into the IR cell containing the MOF by bubbling helium carrier gas through liquid methanol). The IR spectrum (Supporting Information, Figure S2) indicates the presence of the expected physisorbed methanol on UiO-66, as judged by new IR bands at 2945 and 2841 cm^{-1}, which match closely those observed for methanol physisorbed on zirconia powder and those observed for methanol vapor.[34]

To gain further insight into the nature of the methanol substitution process, potential structures and their relative free energies were computed from density functional theory (M06-L functional, see the Methods section for computational details). As illustrated in Figure 3, the thermodynamically most favorable structure is **2**, which is formed through the substitution of one water molecule by one methanol molecule followed by the loss of the terminating hydroxide as a second water molecule after abstraction of the coordinated methanol proton. (Note that the loss of two equivalents of water becomes still more favorable with methanol containing less than the 1% water that was assumed simply as a convenient standard-state condition.) Structure **2** is predicted to be more stable relative to the adsorption of a second methanol molecule (tautomeric structures **3** and **4**), even in liquid methanol.

Computed C−H stretching vibrations for the OCH_3 group in **2**, after the application of a scaling factor of 0.958 (a standard value for M06-L[35]), occur at 2913 and 2812 cm^{-1}; these compare favorably with the experimental values of 2932 and 2828 cm^{-1} (three peaks are computed for the relevant C−H stretches, the symmetric stretch with strong intensity at lower frequency, and two asymmetric stretches, one with strong and one with weak intensity, respectively—experiment does not resolve these two peaks and we take the lowest of the computed values, which provides a peak separation most consistent with the two peaks observed experimentally). With respect to structure **3**, which the calculations show to be energetically less favorable, a vibration is predicted at 2618 cm^{-1} for the stretch of the methanol OH group hydrogen bonded to the adjacent methoxide; no such stretch was observed experimentally.

Extending the work from UiO-66 to NU-1000, we conducted similar methanol washing experiments and obtained the IR

DOI: 10.1021/jacs.6b08273
J. Am. Chem. Soc. 2016, 138, 15189−15196

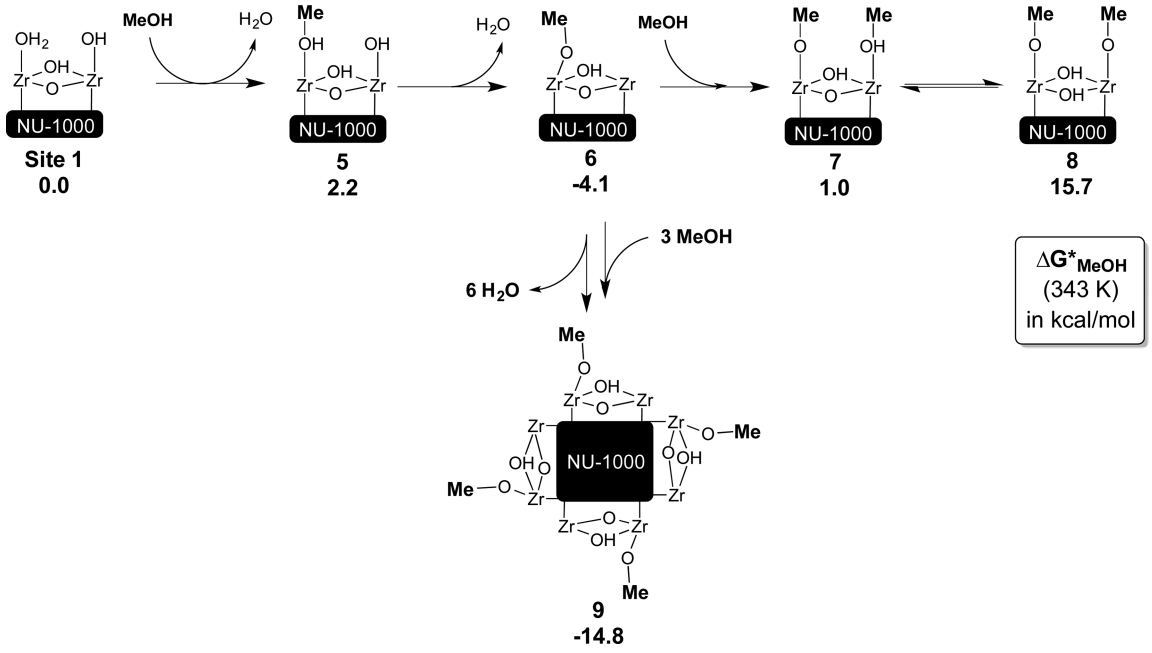

Figure 5. Relative free energies (343 K, liquid methanol, MeOH, containing 1% H_2O) of possible products from methanol substitution. Only one face of NU-1000 was modified in the calculations on the upper line. Consistent with prior work indicating little communication between faces with respect to thermochemical changes associated with node decoration, the energy predicted for structure **9**, having the topology of **6** on all four NU-1000 faces (−14.8 kcal mol^{-1}), is just slightly less than 4 times the value for a single face.

spectra in Figure 4. The sharp band at 2746 cm^{-1} observed for pre-methanol-washed NU-1000 (spectrum **a**) is similar to that found for pre-methanol-washed UiO-66 modulated with HCl and washed with acetone, and it is similarly assigned[4,16] to the hydrogen-bonded OH/OH_2 stretch associated with **site 1**. We soaked this NU-1000 in neat methanol at 343 K for 48 h and then removed the methanol under high vacuum at 298 K followed by further high-vacuum treatment at 423 K, avoiding contact with moisture at all steps. Following these treatments, the band characterizing the hydrogen-bonded OH/OH_2 species, at 2746 cm^{-1}, disappeared, and two new bands appeared, at 2928 and 2825 cm^{-1} (Figure 4, spectrum **b**), again attributed to methoxy group C−H stretches as observed for UiO-66. Simultaneously, the band at 3674 cm^{-1}, assigned to non-hydrogen-bonded μ_3-OH and OH and OH_2 stretches,[4,16] disappeared, with a new, broader band appearing, centered at 3657 cm^{-1}, which we assign to the μ_3-OH stretches in the newly formed surface species. Furthermore, a band was observed at 1155 cm^{-1}, which we associate with the ν_{CO} stretch of the methoxy group. (We note that up to 30−50% of the methoxy groups adsorbed on bulk zirconia are observed to be coordinated in a μ_2 fashion to two zirconium atoms,[28,29] as judged by a lower-frequency ν_{CO} stretch observed in the spectrum of the bulk. In spectrum **b**, we observe a very low-intensity peak at 1039 cm^{-1} that might possibly be attributed to such a species, but DFT does not find such a structure to be stationary, and thus we infer that, if such species were present, they must be at very low concentration, and that the different local environment of the MOF node compared with a bulk zirconia surface mitigates their formation.)

The same computational procedure described above for UiO-66 was employed to characterize the effect of methanol washing on NU-1000, and analogously to structure **2**, structure **6** was found again to be the most thermodynamically favored species in contact with methanol solution (Figure 5). For the structure having the topology of **6** on all four NU-1000 faces (Figure 5, structure **9**), the peaks associated with methoxy group C−H bond stretching are computed to occur at 2927 and 2847 cm^{-1}, again in satisfactory agreement with the experimental values. The computed ν_{CO} stretch **9** is found at 1129 cm^{-1} (averaged over peaks with strong C−O stretching character separated by 26 cm^{-1}), whereas the corresponding peak for the less stable **7** (when considering substitution on a single face) is predicted to be on average at 1049 cm^{-1}; the former value is in considerably better agreement with experiment than the latter, supporting the inference of the predominant presence of the topology of **6** on each face (i.e., **9**) after washing and activation of the MOF.

In additional experiments, we observed that the reaction between methanol and hydroxyl groups on NU-1000 nodes also takes place at 298 K, as by the results of Figure S3 in the Supporting Information, but the conversion under these conditions was incomplete.

We tested the reactivity of node-surface-bound methoxy groups with water, finding that the treatment generated **site 2**. After treatment of the UiO-66 sample that had been exposed to methanol at 298 K for 48 h and the NU-1000 sample that had been exposed to methanol at 343 K for 48 h with water vapor at 393 K for 30 min (water vapor was introduced into the IR cell containing the MOF by bubbling helium carrier gas through liquid water), the bands in the IR spectrum characterizing the C−H vibrations at 2932 and 2828 cm^{-1} for UiO-66 and the C−H vibrations at 2928 and 2825 cm^{-1} and the C−O vibration at 1155 cm^{-1} for NU-1000 decreased substantially (Figure 2c and Figure 4c).

Moreover, a new band was observed at 3781 cm^{-1}, indicating the presence of new terminal OH groups. Methanol produced in the reaction of the methoxy groups with water was observed in the effluent gas by mass spectrometry (Figure S5, Supporting Information). Having calibrated our mass spectrometer with

DOI: 10.1021/jacs.6b08273
J. Am. Chem. Soc. 2016, 138, 15189−15196

pulses of methanol, we determined how much methanol desorbed as a result of the reaction with water, finding the number of methoxy groups per NU-1000 node to be 3.9. Thus, the number of missing linker sites calculated from the quantified methanol signal (assuming only one methoxy group is bonded to each missing linker site per UiO-66 node), 1.84/12, is in good agreement with the value of 1.75/12 determined by thermogravimetric analysis of the MOF.[36] Consequently, we conclude that structure **2** and structure **9** is an accurate representation of the structure for UiO-66 and for NU-1000 after the methanol treatment, respectively.

The methoxy groups are evidently needed as intermediate species to facilitate the conversion from **site 1** to **site 2** on the node vacancies. When we treated UiO-66 or NU-1000 samples incorporating **site 1** with just water in a closed container at 393 K for 12 h, there was no observed conversion of **site 1**. Nor was **site 2** converted to **site 1** under such conditions.

The calculated IR spectra of NU-1000 structures **6**, **9**, one monohydroxy-substituted NU-1000 **site 2**, and a NU-1000 fully substituted with four **sites 2** (designated as **10**) are presented in Figure 4. A peak at about 3727 cm^{-1} was observed for **10**, representing the O−H stretching, which is 54 cm^{-1} blue-shifted compared with the experimental value of 3781 cm^{-1}. The μ_3-O−H stretching is observed at about 3673 cm^{-1} for **6**, NU-1000 **site 2**, and **10**, whereby the structure **6** band is in good agreement with Figure 4.A.a, which represents the MOF after methanol treatment at 298.15 K. A difference of 22 cm^{-1} was observed for NU-1000 **site 2** and **10**. For details, see Table S5 in the Supporting Information.

CM5 partial charge analysis was performed for the Zr_6 nodes having **site 1** and **site 2** topologies, as well as for structures **2**, **6**, and **10** (Table S2). The charge increase for the low-coordinate Zr in UiO-66 is +0.05 au on going from **site 1** to structure **2** and +0.07 au on going from **site 1** to **site 2**. For NU-1000, the same change of +0.07 au was observed, both on going from **site 1** to structure **5** and also at every undercoordinated Zr on going from **site 1** to **10**. As might be expected, eliminating an aqua ligand increases the electrophilicity of the undercoordinated metal atom in every instance.

To generalize the chemistry, we used ethanol or 1-propanol instead of methanol in the reaction with **site 1** on UiO-66 nodes, with the results in Figures S6 and S7 in the Supporting Information. The C−H bands for ethoxy groups appear in the respective IR spectra at 2972, 2930, and 2871 cm^{-1}, and these disappeared after contact of the ethoxylated sample with water vapor at 423 K for 1 h, with a simultaneous increase in the 3780 cm^{-1} band characterizing **site 2**. The C−H bands for *n*-propoxy groups appeared in the IR spectrum at 2962, 2932, 2877, and 2859 cm^{-1}. In contrast to methoxy and ethoxy groups, the propoxy groups were not removed by the water vapor treatment at 423 K for 3 h, and we speculate that the lack of reactivity in this instance may be an indication that the alkyl chain of 1-propanol is sufficiently long for favorable van der Waals interactions with the surrounding organic linkers to reduce its effective volatility compared with those of methanol and ethanol.

DISCUSSION

The chemistry associated with these various face topology changes on the Zr_6 nodes is represented in Scheme 2. We emphasize that the methanol (or ethanol) treatment is crucial for the conversion of **site 1** to **site 2** at moderate temperature, as treatment of either UiO-66 or NU-1000 with water or

Scheme 2. Chemistry Inferred for Face Topology Changes on the MOF Zr_6 Nodes

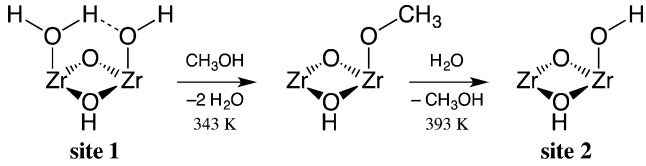

helium or exposure to high vacuum at 393 K does not lead to loss of the aqua ligand, although treatment at temperatures above 473 K with the sample under high vacuum does effect conversion (Figure S8, Supporting Information). Considering the reverse reaction, we observed that **site 2** is not converted to **site 1** by treatment with water at various temperatures, at least over shorter time scales.

That the aqua ligand of **site 1** is not lost upon treatment with hot water is perhaps not surprising, particularly given that the gas-phase binding enthalpy of the aqua ligand to Zr in **site 1** is predicted to be 34 and 38 kcal/mol in UiO-66 and NU-1000, respectively. Soaking of the sample in alcohol, however, permits an equilibrium exchange driven by concentration differences (and favorable solvation of lost water) that permits access to the monoalkoxy substituted facial topology (structures **2** and **6** in Figures 3 and 5, respectively), and, in contrast to the situation in water, binding of an additional neutral alcohol is *not* predicted to be favorable. This reasoning sets up a scenario whereby subsequent water treatment reverses the concentration imbalance, and swapping of hydroxide for methoxide is computed to be almost thermoneutral on conversion to a local **site 2**. What is puzzling, of course, is that treatment of **site 2** with high-temperature water does not lead to speedy regeneration of **site 1**. It may be that the hydrophobic nature of the local environment in contact with the MOF face, which derives from the proximity of the aromatic linkers, leads to a local aqueous structure that is clathrate-like, and that such structuring makes it energetically difficult for a water molecule near the face to recoordinate to Zr. Assessing such a situation would require simulations with explicit solvent (and a suitable model for computing Zr−O interactions) that go beyond the scope of this work, but this is a topic meriting further study. It *is* known that fully dehydrated NU-1000 reverts to fully hydrated NU-1000 (i.e., all faces having **site 1** topology) when exposed to benchtop humidity for a period of several weeks,[37] and, thus, we are confident that the barrier is indeed kinetic in nature.

The chemistry reported here is unique to MOFs because the conversion involves unique terminal OH and/or OH_2 groups on MOF nodes, and comparable groups are evidently lacking in zeolites and metal oxides. The uniform structures of the MOFs allow unprecedentedly precise control of surfaces with these groups, which are essential for some separations by adsorption,[9] for catalysis,[38,39] and for anchoring of metal complexes.[4,5,40]

We note, however, that the ν_{OH} bands of terminal OH groups of **site 2** on UiO-66 and NU-1000 have full width at half-maximum (fwhm) values of about 26 and 23 cm^{-1}, respectively. In contrast, the value characterizing the hydroxyl band at 3630 cm^{-1} in the IR spectrum of SiOHAl groups of HY zeolite (Figure S9 in the Supporting Information) is only 9 cm^{-1}. A comparison of these values indicates that the degree of uniformity of hydroxyl **sites 2** on the Zr_6 MOF nodes is markedly less than the degree of uniformity of comparable hydroxyl sites on the zeolite, consistent with our previously reported results derived from the fwhm values characterizing

DOI: 10.1021/jacs.6b08273
J. Am. Chem. Soc. 2016, 138, 15189−15196

ν_{CO} bands of $Ir(CO)_2$ species anchored to the MOF nodes and to HY zeolite.[4] There is more yet to be learned about the subtle chemistry of these MOF nodes and their surface sites.

CONCLUSIONS

In summary, methoxy groups on the Zr_6 nodes of UiO-66 and NU-1000 (Scheme 1), characterized by IR bands at 2932 and 2828 cm^{-1} and identified by IR spectroscopy and DFT calculations, arise from the reaction of the MOF node hydrogen-bonded OH/OH_2 groups (**site 1**) with methanol, and the resultant node surface structure is converted into one vacant Zr site and one terminal OH group upon reaction with water. To the best of our knowledge, this is the first example of the tuning of the chemistry of reactive groups (hydroxyl groups) on MOF nodes—and the intermediacy of methoxy or ethoxy groups is crucial for control of this chemistry. Because the DFT calculations demonstrate that the various types of hydroxyl groups on the Zr_6 nodes have markedly different properties, and because these groups perform differently from each other in bonding to metal complexes,[4,5] we may expect the control of these sites to open precise new chemistry, including that of anchored metal complexes, on MOF nodes.

ASSOCIATED CONTENT

Supporting Information

The Supporting Information is available free of charge on the ACS Publications website at DOI: 10.1021/jacs.6b08273.

Experimental and computational details, primarily IR spectra and Cartesian coordinates with their associated energies (PDF)

AUTHOR INFORMATION

Corresponding Authors

*gagliard@umn.edu

*bcgates@ucdavis.edu

Notes

The authors declare no competing financial interest.

ACKNOWLEDGMENTS

This work was supported as part of the Inorganometallic Catalyst Design Center, an Energy Frontier Research Center funded by the U.S. Department of Energy, Office of Science, Basic Energy Sciences, under Award DE-SC0012702.

REFERENCES

(1) Cavka, J. H.; Jakobsen, S.; Olsbye, U.; Guillou, N.; Lamberti, C.; Bordiga, S.; Lillerud, K. P. *J. Am. Chem. Soc.* **2008**, *130*, 13850−13851.

(2) Mondloch, J. E.; Bury, W.; Fairen-Jimenez, D.; Kwon, S.; DeMarco, E. J.; Weston, M. H.; Sarjeant, A. A.; Nguyen, S. T.; Stair, P. C.; Snurr, R. Q.; Farha, O. K.; Hupp, J. T. *J. Am. Chem. Soc.* **2013**, *135*, 10294−10297.

(3) Nguyen, H. G. T.; Schweitzer, N. M.; Chang, C. Y.; Drake, T. L.; So, M. C.; Stair, P. C.; Farha, O. K.; Hupp, J. T.; Nguyen, S. T. *ACS Catal.* **2014**, *4*, 2496−2500.

(4) Yang, D.; Odoh, S. O.; Borycz, J.; Wang, T. C.; Farha, O. K.; Hupp, J. T.; Cramer, C. J.; Gagliardi, L.; Gates, B. C. *ACS Catal.* **2016**, *6*, 235−247.

(5) Yang, D.; Odoh, S. O.; Wang, T. C.; Farha, O. K.; Hupp, J. T.; Cramer, C. J.; Gagliardi, L.; Gates, B. C. *J. Am. Chem. Soc.* **2015**, *137*, 7391−7396.

(6) Cliffe, M. J.; Wan, W.; Zou, X. D.; Chater, P. A.; Kleppe, A. K.; Tucker, M. G.; Wilhelm, H.; Funnell, N. P.; Coudert, F. X.; Goodwin, A. L. *Nat. Commun.* **2014**, *5*, 4176/1−4176/8.

(7) Shearer, G. C.; Chavan, S.; Bordiga, S.; Svelle, S.; Olsbye, U.; Lillerud, K. P. *Chem. Mater.* **2016**, *28*, 3749−3761.

(8) Cheetham, A. K.; Bennett, T. D.; Coudert, F. X.; Goodwin, A. L. *Dalton Trans.* **2016**, *45*, 4113−4126.

(9) Jiang, J. C.; Yaghi, O. M. *Chem. Rev.* **2015**, *115*, 6966−6997.

(10) Klet, R. C.; Liu, Y. Y.; Wang, T. C.; Hupp, J. T.; Farha, O. K. *J. Mater. Chem. A* **2016**, *4*, 1479−1485.

(11) Yuan, S.; Chen, Y. P.; Qin, J. S.; Lu, W. G.; Wang, X.; Zhang, Q.; Bosch, M.; Liu, T. F.; Lian, X. Z.; Zhou, H. C. *Angew. Chem., Int. Ed.* **2015**, *54*, 14696−14700.

(12) Klet, R. C.; Tussupbayev, S.; Borycz, J.; Gallagher, J. R.; Stalzer, M. M.; Miller, J. T.; Gagliardi, L.; Hupp, J. T.; Marks, T. J.; Cramer, C. J.; Delferro, M.; Farha, O. K. *J. Am. Chem. Soc.* **2015**, *137*, 15680−15683.

(13) Madrahimov, S. T.; Gallagher, J. R.; Zhang, G. H.; Meinhart, Z.; Garibay, S. J.; Delferro, M.; Miller, J. T.; Farha, O. K.; Hupp, J. T.; Nguyen, S. T. *ACS Catal.* **2015**, *5*, 6713−6718.

(14) Ling, S. L.; Slater, B. *Chem. Sci.* **2016**, *7*, 4706−4712.

(15) Trickett, C. A.; Gagnon, K. J.; Lee, S.; Gandara, F.; Burgi, H. B.; Yaghi, O. M. *Angew. Chem., Int. Ed.* **2015**, *54*, 11162−11167.

(16) Planas, N.; Mondloch, J. E.; Tussupbayev, S.; Borycz, J.; Gagliardi, L.; Hupp, J. T.; Farha, O. K.; Cramer, C. J. *J. Phys. Chem. Lett.* **2014**, *5*, 3716−3723.

(17) Deria, P.; Bury, W.; Hupp, J. T.; Farha, O. K. *Chem. Commun.* **2014**, *50*, 1965−1968.

(18) Deria, P.; Mondloch, J. E.; Tylianakis, E.; Ghosh, P.; Bury, W.; Snurr, R. Q.; Hupp, J. T.; Farha, O. K. *J. Am. Chem. Soc.* **2013**, *135*, 16801−16804.

(19) Deria, P.; Bury, W.; Hod, I.; Kung, C. W.; Karagiaridi, O.; Hupp, J. T.; Farha, O. K. *Inorg. Chem.* **2015**, *54*, 2185−2192.

(20) Wang, T. C.; Vermeulen, N. A.; Kim, I. S.; Martinson, A. B. F.; Stoddart, J. F.; Hupp, J. T.; Farha, O. K. *Nat. Protoc.* **2016**, *11*, 149−162.

(21) Marenich, A. V.; Jerome, S. V.; Cramer, C. J.; Truhlar, D. G. *J. Chem. Theory Comput.* **2012**, *8*, 527−541.

(22) Zhao, Y.; Truhlar, D. G. *J. Chem. Phys.* **2006**, *125*, 194101/1−194101/17.

(23) Frisch, M. J.; Trucks, G. W.; Schlegel, H. B.; Scuseria, G. E.; Robb, M. A.; Cheeseman, J. R.; Scalmani, G.; Barone, V.; Mennucci, B.; Petersson, G. A.; Nakatsuji, H.; Caricato, M.; Li, X.; Hratchian, H. P.; Izmaylov, A. F.; Bloino, J.; Zheng, G.; Sonnenberg, J. L.; Hada, M.; Ehara, M.; Toyota, K.; Fukuda, R.; Hasegawa, J.; Ishida, M.; Nakajima, T.; Honda, Y.; Kitao, O.; Nakai, H.; Vreven, T.; Montgomery, J. J. A.; Peralta, J. E.; Ogliaro, F.; Bearpark, M.; Heyd, J. J.; Brothers, E.; Kudin, K. N.; Staroverov, V. N.; Kobayashi, R.; Normand, J.; Raghavachari, K.; Rendell, A.; Burant, J. C.; Iyengar, S. S.; Tomasi, J.; Cossi, M.; Rega, N.; Millam, J. M.; Klene, M.; Knox, J. E.; Cross, J. B.; Bakken, V.; Adamo, C.; Jaramillo, J.; Gomperts, R.; Stratmann, R. E.; Yazyev, O.; Austin, A. J.; Cammi, R.; Pomelli, C.; Ochterski, J. W.; Martin, R. L.; Morokuma, K.; Zakrzewski, V. G.; Voth, G. A.; Salvador, P.; Dannenberg, J. J.; Dapprich, S.; Daniels, A. D.; Farkas, Ö.; Foresman, J. B.; Ortiz, J. V.; Cioslowski, J.; Fox, D. J. *Gaussian 09*, revision A.02; Gaussian, Inc.: Wallingford, CT, 2009.

(24) Weigend, F. *Phys. Chem. Chem. Phys.* **2006**, *8*, 1057−1065.

(25) Weigend, F.; Ahlrichs, R. *Phys. Chem. Chem. Phys.* **2005**, *7*, 3297−3305.

(26) Marenich, A. V.; Cramer, C. J.; Truhlar, D. G. *J. Phys. Chem. B* **2009**, *113*, 6378−6396.

(27) Katz, M. J.; Brown, Z. J.; Colon, Y. J.; Siu, P. W.; Scheidt, K. A.; Snurr, R. Q.; Hupp, J. T.; Farha, O. K. *Chem. Commun.* **2013**, *49*, 9449−9451.

(28) Ouyang, F.; Kondo, J. N.; Maruya, K.; Domen, K. *J. Phys. Chem. B* **1997**, *101*, 4867−4869.

(29) June, K. T.; Bell, A. T. *J. Catal.* **2001**, *204*, 339−347.

(30) Beebe, T. P.; Crowell, J. E.; Yates, J. T. *J. Phys. Chem.* **1988**, *92*, 1296−1301.

(31) Busca, G.; Lorenzelli, V. *J. Catal.* **1980**, *66*, 155−161.

(32) Morrow, B. A. *J. Chem. Soc., Faraday Trans. 1* **1974**, *70*, 1527−1545.

DOI: 10.1021/jacs.6b08273
J. Am. Chem. Soc. 2016, 138, 15189−15196

(33) June, K. D.; Bell, A. T. *J. Catal.* **2000**, *193*, 207−223.
(34) Plyler, E. K. *J. Res. Natl. Bur. Stand.* **1952**, *48*, 281−286.
(35) Alecu, I. M.; Zheng, J.; Zhao, Y.; Truhlar, D. G. *J. Chem. Theory Comput.* **2010**, *6*, 2872−2887.
(36) Liu, Y. Y.; Klet, R. C.; Hupp, J. T.; Farha, O. *Chem. Commun.* **2016**, *52*, 7806−7809.
(37) Mondloch, J. E.; Katz, M. J.; Isley, W. C.; Ghosh, P.; Liao, P. L.; Bury, W.; Wagner, G.; Hall, M. G.; DeCoste, J. B.; Peterson, G. W.; Snurr, R. Q.; Cramer, C. J.; Hupp, J. T.; Farha, O. K. *Nat. Mater.* **2015**, *14*, 512.
(38) Corma, A.; Garcia, H.; Xamena, F. X. L. I. *Chem. Rev.* **2010**, *110*, 4606−4655.
(39) Katz, M. J.; Klet, R. C.; Moon, S. Y.; Mondloch, J. E.; Hupp, J. T.; Farha, O. K. *ACS Catal.* **2015**, *5*, 4637−4642.
(40) Manna, K.; Ji, P. F.; Greene, F. X.; Lin, W. B. *J. Am. Chem. Soc.* **2016**, *138*, 7488−7491.

DOI: 10.1021/jacs.6b08273
J. Am. Chem. Soc. 2016, 138, 15189−15196